Weak antilocalization in HgTe quantum wells with inverted energy spectra

G. M. Minkov,[1,2] A. V. Germanenko,[2] O. E. Rut,[2] A. A. Sherstobitov,[1,2] S. A. Dvoretski,[3] and N. N. Mikhailov[3]
[1]*Institute of Metal Physics, 620990 Ekaterinburg, Russia*
[2]*Institute of Natural Sciences, Ural Federal University, 620000 Ekaterinburg, Russia*
[3]*Institute of Semiconductor Physics, 630090 Novosibirsk, Russia*
(Received 15 February 2012; revised manuscript received 28 April 2012; published 14 June 2012)

The results of an experimental study of the magnetoconductivity of two-dimensional (2D) electron gas caused by suppression of the interference quantum correction in a HgTe single quantum well heterostructure with an inverted energy spectrum are presented. It is shown that only the antilocalization magnetoconductivity is observed at relatively high conductivity, $\sigma > (20\text{–}30)\,G_0$, where $G_0 = e^2/2\pi^2\hbar$. The antilocalization correction demonstrates a crossover from $0.5\,\ln(\tau_\phi/\tau)$ to $1.0\,\ln(\tau_\phi/\tau)$ behavior with increasing conductivity (here τ_ϕ and τ are the phase relaxation and transport relaxation times, respectively). It is interpreted as a result of crossover to the regime when the two chiral branches of the electron energy spectrum independently contribute to the weak antilocalization. At lower conductivity, $\sigma < (20\text{–}30)\,G_0$, the magnetoconductivity behaves similarly to that in usual 2D systems with fast spin relaxation: It is negative in low magnetic fields and positive in higher ones. We have found that the temperature dependences of the fitting parameter τ_ϕ corresponding to the phase relaxation time demonstrate reasonable behavior, close to $1/T$, over the whole conductivity range from $5\,G_0$ up to $130\,G_0$. However, the τ_ϕ value remains practically independent of conductivity, in contrast to conventional 2D systems with simple energy spectra, in which τ_ϕ is enhanced with conductivity.

DOI: 10.1103/PhysRevB.85.235312 PACS number(s): 73.20.Fz, 73.61.Ey

I. INTRODUCTION

A type of two-dimensional (2D) system in which the energy spectrum is formed by the spin-orbit interaction has attracted considerable interest during the past decade. In these structures, the Dirac-like spectrum is realized. This leads to the appearance of new dependences and modification of traditional dependences of kinetic phenomena on the magnetic field, temperature, carrier density, and so forth. Graphene,[1,2] topological insulators such as $Bi_{1-x}Sb_x$, Bi_2Se_3, and Bi_2Te_3,[3,4] and quantum wells of gapless semiconductor HgTe[5,6] belong to this type of the system. A unique property of the band structure of HgTe caused by strong spin-orbit interaction is the energetic inversion of the Γ_6 and Γ_8 ordering proposed in Ref. 7 to explain the properties of gray tin. It results in the appearance of interface states,[8–10] which cause nontrivial dependence of the energy gap on the width d of the HgTe-quantum well,[11] and other significant features of the energy spectrum of these systems. It is illustrated by Fig. 1, where the energy of subbands of size quantization at $k = 0$ is plotted as a function of the HgTe quantum well width for the $Hg_{0.35}Cd_{0.65}Te$/HgTe heterostructure. The subbands formed from the Γ_8 heavy hole states are labeled as h1, h2, ..., while the subbands formed from the Γ_8 electron states are labeled as e1, e2, ... The subband s1 originates from the interface state[11] and is formed by coupling of the Γ_6 states with light Γ_8 states. When the width is relatively large, $d \gtrsim 7.5$ nm, the energy gap is formed by the bands h1 and h2 but not by the bands $e1$ and h1, as would be naively expected when considering the electron and hole bands independently. Another peculiar feature of the spectrum is the existence of critical width d_c corresponding to the collapse of the energy gap, in which the band ordering changes from inverted at $d > d_c$ nm to the normal one at $d < d_c$.[5] In the vicinity of d_c the Dirac-like spectrum, which has attracted considerable interest in recent years, is realized. Much progress in $Hg_{1-x}Cd_xTe$/HgTe heterostructures[12,13] raises the possibility of carrying out detailed studies of the transport phenomena in such 2D systems. Many papers have been devoted to the study of high magnetic field transport,[14–16] the quantum Hall effect,[17,18] and crossover from electron to hole conductivity in the gated structures.[19,20] At the same time, effects resulting from the quantum interference were investigated in solely experimental[21] and solely theoretical[22] papers.

In this work, we present the results of experimental study of the interference quantum correction to the conductivity ($\delta\sigma$) in the HgTe single quantum well with the inverted energy spectrum. It is shown that only the antilocalization magnetoconductivity is observed at relatively high conductivity $\sigma > (20\text{–}30)\,G_0$, where $G_0 = e^2/2\pi^2\hbar$. The antilocalization correction demonstrates a crossover from the regime when $\delta\sigma = -\alpha\,\ln(\tau_\phi/\tau)$ with $\alpha = -0.5$ to that with $\alpha = -1.0$ (τ_ϕ and τ are the phase relaxation and transport relaxation times, respectively). It is interpreted as a crossover to the regime when the two chiral branches of the energy spectrum independently contribute to the weak antilocalization. At lower conductivity $\sigma < (20\text{–}30)\,G_0$, the magnetoconductivity behaves similarly to that in usual 2D systems with fast spin relaxation. The magnetoconductivity curves in this case are well fitted by the standard expression.[24,25] We find that the temperature dependence of τ_ϕ, whose value is found from the fit, is close to $1/T$ as it should be when the inelasticity of electron-electron (e-e) interaction is the main mechanism of phase relaxation.[26] At the same time, the τ_ϕ value remains practically independent of the conductivity, in contrast to the ordinary 2D systems, where τ_ϕ is roughly proportional to the conductivity.

II. EXPERIMENTAL

Our HgTe quantum wells were realized on the basis of $HgTe/Hg_{1-x}Cd_xTe$ ($x = 0.5\text{–}0.65$) heterostructure grown by means of molecular beam epitaxy on a GaAs substrate with

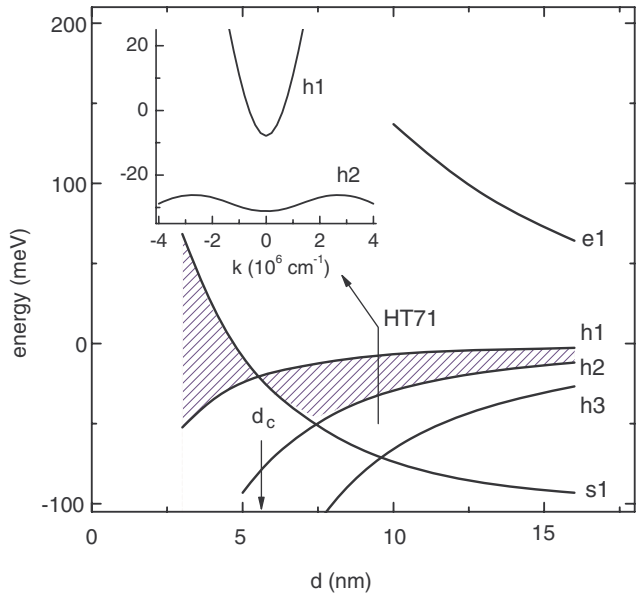

FIG. 1. (Color online) Energies of subbands at $k = 0$ as a function of the HgTe quantum well width for the $Hg_{0.35}Cd_{0.65}Te/HgTe/Hg_{0.35}Cd_{0.65}Te$ heterostructure calculated in the 6×6 **kP** model with the use of the direct integration technique as described in Ref. 23. The widths of $Hg_{0.35}Cd_{0.65}Te/HgTe$ interfaces were equal to 1 nm, and other band parameters were the same as in Ref. 17. The dashed area indicates the energy gap at $k = 0$. The subbands are labeled in accordance with Ref. 11. The inset shows the dispersion law for $d = 9.5$ nm corresponding to the structure HT71.

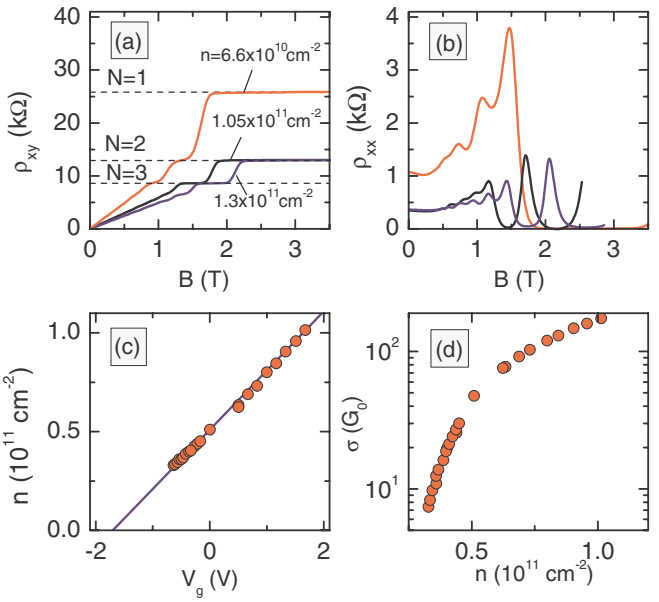

FIG. 2. (Color online) Magnetic field dependences of (a) ρ_{xy} and (b) ρ_{xx}, measured at $T = 1.35$ K for the different electron densities. (c) Gate voltage dependences of the electron densities found as $n = 1/(eR_H)$ at $B = 0.1$ T. Symbols plot the data, and the line shows the dependence $n = CV_g/|e| + 5.1 \times 10^{10}$ cm^{-2} plotted with $C = 4.8$ nF/cm^2 measured experimentally. (d) Conductivity measured at $B = 0$ and $T = 1.35$ K as a function of the electron density.

(013) surface orientation.[13] Three heterostructures HT108, HT71, and H922 with nominal widths of quantum wells equal to 9.0 nm, 9.5 nm, and 10 nm, respectively, were investigated. The energy dispersion of the lowest electron and highest hole subband calculated in the 6×6 isotropic **kP** model for heterostructure HT71 is shown in the inset in Fig. 1. The samples were mesa etched into standard Hall bars. To change and control the electron density (n) in the quantum well, the field-effect transistors were fabricated with parylene as an insulator and aluminium as a gate electrode. In some cases the illumination was used to change the electron density. The conductivity of the structure HT71 after cooling to the liquid helium temperature was very low, $\sigma \simeq 10^{-2}\, G_0$, and enhanced up to $\simeq 130\, G_0$ with the help of illumination or application of the gate voltage (V_g). The electron densities in the structures HT108 and H922 at $V_g = 0$ were about 4.5×10^{11} cm^{-2} and 5.0×10^{11} cm^{-2}, respectively, and were decreased to $(3 - 5) \times 10^{10}$ cm^{-2} by the gate voltage. The electron mobilities at $n = 1.0 \times 10^{11}$ cm^{-2} were 1.3×10^5 cm^2/V s, 4.5×10^4 cm^2/V s, and 4.5×10^4 cm^2/V s in the structures HT71, HT108, and H922, respectively. The main results were analogous for all the structures. For this reason, the figures represent the results obtained on the structure HT71, except as otherwise noted.

III. RESULTS AND DISCUSSION

The magnetic field dependences of off-diagonal and diagonal components of the resistivity tensor (ρ_{xy} and ρ_{xx}) at some gate voltages are presented in Figs. 2(a) and 2(b), respectively. Well-resolved quantum Hall plateaus, both the even and odd, are evident. The V_g dependence of the electron density found as $n = 1/(eR_H)$ at $B = 0.1$ T, where R_H is the Hall coefficient, and the electron density dependence of the conductivity at $T = 1.35$ K are plotted in Figs. 2(c) and 2(d), respectively. As seen, the n vs V_g plot is close to the linear one and its slope corresponds to the geometric capacity $C = 4.8$ nF/cm^2 measured on the same sample.

To interpret the experimental results, we need to know the electron effective mass. The reliable determination of the mass from the Shubnikov–de Haas oscillations was successful for $n = 8 \times 10^{10}$ cm^{-2}. We have obtained $m = (0.022 \pm 0.005)\, m_0$. This value agrees well with the theoretical value $m = 0.019\, m_0$ obtained within the 6×6 **kP** model. The calculations show also that the increase of the effective mass does not exceed 15% when the electron density changes from 3×10^{10} cm^{-2} to 1.5×10^{11} cm^{-2}. For this reason the value $0.022\, m_0$ is used to treat the data over the whole conductivity range.

Let us consider the low field magnetoconductivity presented in Fig. 3. To compare the experimental curves measured at different conductivity values, we plot them against the relative magnetic field $b = B/B_{tr}$, where $B_{tr} = \hbar/2el^2$ with l as the mean free path is the characteristic magnetic field for the interference correction. Furthermore, we shift the experimental curves $\Delta\sigma(b) = 1/\rho_{xx}(b) - 1/\rho_{xx}(0)$ in the vertical direction on the value of the interference correction at $B = 0$, $\delta\sigma(0)$, found as described in Sec. III C. So, the plotted dependence in Fig. 3 is actually the b dependence of the interference correction $\delta\sigma(b)$. One can see that only the negative (antilocalizing) magnetoconductivity is observed at high conductivity $\sigma > (20\text{–}30)\, G_0$ over the magnetic field

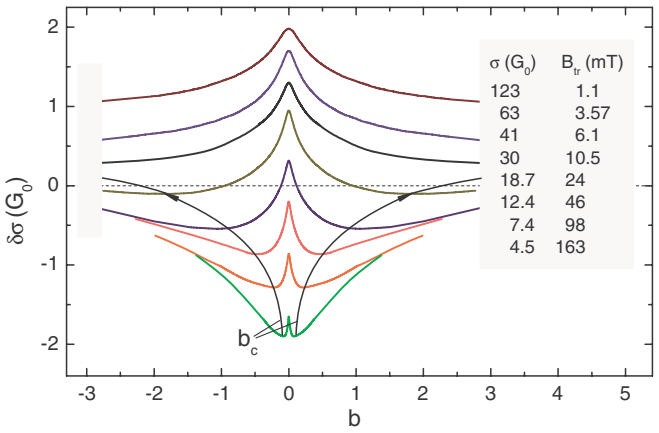

FIG. 3. (Color online) The dependences $\delta\sigma(b) = \Delta\sigma(b) + \delta\sigma(0)$ for different conductivity values, $T = 1.35$ K. The arrows show the shift of the minimum with increasing conductivity.

range up to $b = 3$. At lower conductivity values, the crossover to the positive magnetoconductivity is observed at the magnetic field labeled as b_c. As clearly seen from the figure, as the conductivity becomes lower the value of b_c also becomes lower. At $\sigma < 20\,G_0$ the value of b_c becomes less than unity.

A. Low-field positive magnetoconductivity, high conductivity $\sigma > 20\,G_0$

As far as we know, the theory of interference-induced magnetoconductivity for systems with complicated energy spectra like HgTe quantum wells is not developed yet. Therefore, our analysis leans upon the Dirac model of the energy spectrum. This model is widely used to describe the energy dispersion of s1 and h1 subbands near the critical width d_c.[5] The subbands s1 and h1 at $d \sim d_c$ consist of two branches of different chirality (in what follows they are referred to as k^+ and k^-), which are degenerate in a symmetric quantum well or can be split off due to spin-orbit interaction in the asymmetric case. Although the thickness of the HgTe layer in our samples, $d =$ (9–10) nm, is larger than d_c and the gap is already formed by the subbands h1 and h2 but not by s1 and h1 (see Fig. 1), we suppose that the main features of the electron subband h1 are qualitatively the same as at $d \sim d_c$. The chiral fermions cannot be backscattered and the magnetoconductivity in such heterostructures should demonstrate the antilocalizing behavior. The contribution to the interference correction coming from each branch is positive and equal to $0.5\,G_0 \ln(\tau_\phi/\tau)$, $\tau_\phi \gg \tau$. When the transition rate $1/\tau_\pm$ between the branches k^+ and k^- is small as compared with the phase relaxation rate $1/\tau_\phi$, the interference contributions to the conductivity from these brunches are summarized and the total correction should be equal to $(0.5 + 0.5)\,G_0 \ln(\tau_\phi/\tau)$. In the opposite case, when $1/\tau_\pm \gg 1/\tau_\phi$, the correction should be equal to $0.5\,G_0 \ln(\tau_\phi/\tau)$. So, the interference correction at $B = 0$ for arbitrary relationship between τ_ϕ and $\tau_\pm$ should be equal to

$$\delta\sigma = -\alpha\,G_0 \ln\left(\frac{\tau_\phi}{\tau}\right), \quad -1 \leqslant \alpha \leqslant -0.5. \tag{1}$$

The magnetoconductivity resulting from the suppression of the electron interference by the magnetic field should be described

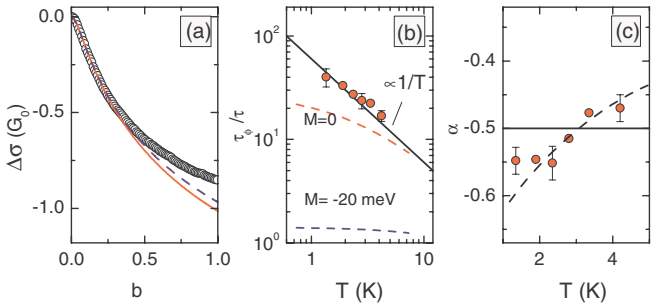

FIG. 4. (Color online) (a) Magnetic field dependence of $\Delta\sigma$ for $n = 5.8 \times 10^{10}$ cm^{-2}, $\sigma = 63\,G_0$, $T = 1.35$ K. Symbols are experimental data. Solid and dashed lines are calculated from Eq. (2) with parameters $\alpha = -0.57$, $\tau_\phi/\tau = 38.5$ (solid curve), and $\alpha = -0.52$, $\tau_\phi/\tau = 41.8$ (dashed curve) corresponding to the best fit made within two fitting intervals $0 < b < 0.2$ and $0 < b < 0.3$, respectively. Temperature dependences of (b) τ_ϕ/τ and (c) α, respectively, found from the fit of the magnetoconductivity curves. The dashed curves in panel (b) are calculated as described in Sec. III A. The dashed line in panel (c) is provided as a guide to the eye; the solid line is $\alpha = -0.5$. Hereafter the error bars indicate the scatter in the data obtained from the different fitting ranges and from different measurements.

by the standard expression[24,25] with the same prefactor α:

$$\Delta\sigma(b) = \alpha\,G_0 \mathcal{H}\left(\frac{\tau}{\tau_\phi}, b\right),$$
$$\mathcal{H}(x,y) = \psi\left(\frac{1}{2} + \frac{x}{y}\right) - \psi\left(\frac{1}{2} + \frac{1}{y}\right) - \ln x, \tag{2}$$

where $\psi(x)$ is the digamma function. We have used this expression to fit each experimental curve with α and τ_ϕ/τ as the fitting parameters. Because Eq. (2) is correct for the diffusion regime (i.e., for $b \ll 1$), the upper limit of the fitting interval was always less than 0.3. As an example, the result of the fitting procedure made within two different magnetic field ranges, $b < 0.2$ and $b < 0.3$, is presented in Fig. 4(a). One can see that Eq. (2) well describes the run of the experimental curve, and it is important that the values of the fitting parameters are practically independent of the fitting interval.

The temperature dependence of the fitting parameter τ_ϕ/τ as shown by Fig. 4(b) is close to the $1/T$ law that corresponds to the inelasticity of e-e interaction as the main mechanism of the phase relaxation.[26] Such temperature dependence of τ_ϕ is observed over the entire conductivity range $20\,G_0 < \sigma < 130\,G_0$.

We now direct our attention to the prefactor [see Fig. 4(c)]. It is seen that the value of α is close to -0.5 and becomes more negative with decreasing temperature. The fact that $|\alpha|$ is less than 0.5 at $T = 4.2$ K can be explained because the condition $\tau_\phi \gg \tau$, under which Eq. (2) works, is not vigorously fulfilled. When this strong inequality is violated, our fitting procedure gives the value of τ_ϕ, which is close to the true one, whereas α occurs to be reduced in magnitude.[27] For the case presented in Fig. 4, the ratio τ_ϕ/τ is about 17 at $T = 4.2$ K and about 40 at $T = 1.35$ K, which should result in reduction of $|\alpha|$ by factors of about 0.7 and 0.8, respectively, so the "true" value of the prefactor corrected for nondiffusion regime is about -0.7 over the whole temperature range. This value is appreciably less

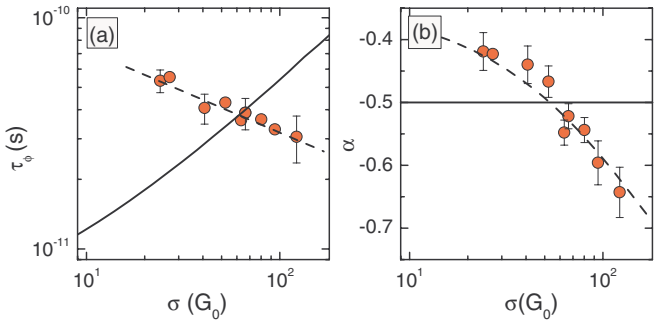

FIG. 5. (Color online) The values of τ_ϕ (a) and α (b) plotted against the conductivity at $T = 1.35$ K. The symbols plot the data. The dashed lines are provided as a guide to the eye. The solid line in panel (a) is calculated in accordance with Ref. 28.

than -0.5, suggesting that our system is in the intermediate regime when the strong inequality $\tau_\pm \gg \tau_\phi$ is not fulfilled yet, and the chiral branches cannot be considered as independent.

Let us next consider the conductivity dependence of τ_ϕ and α shown in Figs. 5(a) and 5(b), respectively. The surprising thing is that the parameter τ_ϕ does not increase with the increasing conductivity as predicted theoretically[28] for the inelasticity of the *e*-*e* interaction as the main mechanism of the phase relaxation [see the solid curve in Fig. 5(a)]. It should be also noted that the value of τ_ϕ found from the fit in HgTe quantum well at $\sigma \simeq 20\,G_0$ is approximately 2.5–3 times as large as the theoretical value of the dephasing time. As Fig. 5(b) demonstrates, the prefactor α increases in magnitude with the increasing conductivity. As discussed above, such the behavior indicates that the interbranch transition time $\tau_\pm$ becomes larger than the dephasing time τ_ϕ, and the 2D gas approaches the regime of the two independent contributions of k^+ and k^- states to the interference quantum correction.

To the best of our knowledge, there is a solely theoretical paper[22] in which the interference correction to the conductivity in HgTe quantum well was studied. According to this paper, the value of the correction at $B = 0$ is

$$\delta\sigma = -2\beta\, G_0 \ln \frac{\tau^{-1}}{\tau_{\mathcal{M}}^{-1} + \tau_\phi^{-1}}, \tag{3}$$

$$\tau_{\mathcal{M}}^{-1} = \frac{2}{\tau} \frac{\left(\mathcal{M} + \mathcal{B}k_F^2\right)^2}{\mathcal{A}^2 k_F^2 + \left(\mathcal{M} + \mathcal{B}k_F^2\right)^2}, \quad k_F = \sqrt{2\pi n}, \tag{4}$$

where $\mathcal{M}$ is the band gap at the Dirac point, $\mathcal{A}$ and $\mathcal{B}$ are the band parameters responsible for the linear and quadratic parts of the energy spectrum, respectively,[5] and $\beta > -1/2$ is the prefactor, which depends on τ/τ_ϕ and $\tau/\tau_{\mathcal{M}}$ so that $\beta \simeq -1/2$ when $\tau/\tau_\phi,\ \tau/\tau_{\mathcal{M}} \ll 1$ [see Eq. (53) in Ref. 22]. Equation (3) is structurally very similar to the conventional expression, Eq. (1), and $1/\tau_\phi + 1/\tau_{\mathcal{M}}$ stands instead of $1/\tau_\phi$. It is natural to suppose that the magnetoconductivity could be described by Eq. (2) with the same substitution. Under this assumption, the fit of the data by Eq. (2) should give $1/\tau_\phi + 1/\tau_{\mathcal{M}}$ instead of $1/\tau_\phi$. However, following this line of attack we are not able to interpret our results. To demonstrate this, we have depicted the temperature dependences of $\tau/(1/\tau_\phi + 1/\tau_{\mathcal{M}})$ calculated for the two $\mathcal{M}$ values, $\mathcal{M} = 0$ and -20 meV, in Fig. 4(b). The parameters $\mathcal{A}$ and $\mathcal{B}$ were equal to 380 meV nm and 850 meV nm^2, respectively, in accordance with Ref. 6, and τ/τ_ϕ varied with the temperature as $\tau/\tau_\phi = 0.014\,T$. One can see that, in contrast to what was observed experimentally, the calculated dependences demonstrate very strong saturation with the temperature decrease, and the saturation is more pronounced for $\mathcal{M} = -20$ meV, which is more appropriate to the structure investigated.

B. Alternative sign magnetoconductivity, $\sigma < 20\,G_0$

Let us analyze the experimental results for the lower conductivity, $\sigma \lesssim 20\,G_0$. In this case, the crossover from the negative magnetoconductivity to the positive one is observed at a magnetic field with a value lower than the transport magnetic field, $b_c = B_c/B_{tr} \lesssim 1$ (see Fig. 3). At first sight $\Delta\sigma(b)$ behaves much like the interference-induced magnetoconductivity observed in conventional 2D systems with fast spin relaxation (see, e.g., Ref. 29). However, the fact that the crossover field B_c is practically independent of the conductivity, $B_c = (15$–$20)$ mT (see Fig. 6), sets one thinking about other possible reasons for the crossover from negative to positive magnetoconductivity at $B = B_c$.

In principle, the positive magnetoconductivity can result from the contribution of the *e*-*e* interaction. It should depend on the magnetic field due to the Zeeman splitting, which suppresses the interaction contribution in the triplet channel.[30–36] If the value of the effective g factor is sufficiently large, the Zeeman splitting $g\mu_B B$, where μ_B stands for the Bohr magneton, can exceed the temperature already in relatively low magnetic field, $B \sim 0.02$ T, and the positive magnetoconductivity resulting from this effect can exceed the negative magnetoconductivity caused by the quantum interference. Our measurements of the interaction correction with the use of the method suggested in Ref. 37 did not reveal any significant magnetic-field dependence of the interaction correction in the actual magnetic-field range. However, it must be admitted that the accuracy of this method at low field is not high enough to assert it unambiguously.

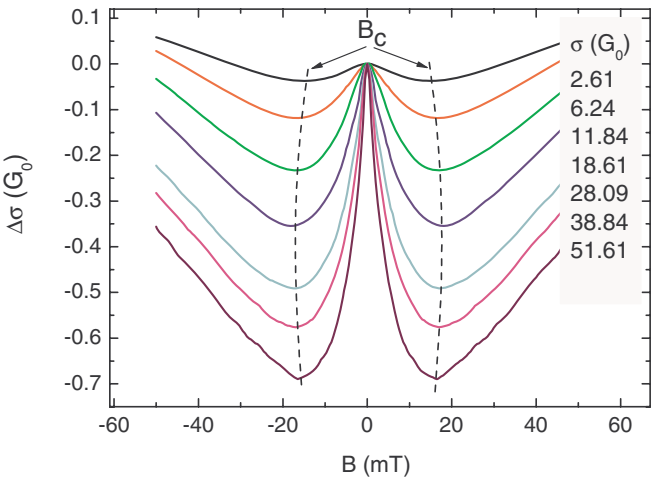

FIG. 6. (Color online) The magnetoconductivity plotted against the magnetic field for different σ at $T = 4.2$ K. The dashed lines demonstrate that the minimum position is practically independent of the conductivity.

Another possible reason for the positive magnetoconductivity is classical memory effects.[38] As shown in Refs. 39 and 40, in which the magnetotransport in the 2D Lorentz gas is studied, the effects due to double scattering of an electron on the same disk lead to a negative magnetoresistance even in classically weak magnetic fields. However, our estimates (made according to Ref. 40 with the use of typical parameters) show that the positive magnetoconductivity due to the memory effect in our case is more than one order of magnitude less than the rise of the magnetoconductivity observed experimentally at $B > B_c$.

So, the known mechanisms of positive magnetoconductivity cannot explain our data. Therefore, despite the fact that the theory does not predict alternative-sign magnetoconductivity for systems with the Dirac-like energy spectrum, let us analyze the data at $\sigma < 20\,G_0$ under assumption that both descending and ascending parts of the magnetoconductivity curves in Figs. 3 and 6 result from suppression of the interference correction by the magnetic field. In what follows, we compare the shape of the magnetoconductivity curve with the well-known expressions employing the standard fitting procedure.

For the case when the spin-orbit splitting of the energy spectrum is cubic in quasimomentum, the magnetoconductivity is described by the Hikami-Larkin-Nagaoka expression[24]

$$\frac{\Delta\sigma(b)}{G_0} = \psi\left(\frac{1}{2}+\frac{\tau}{b}\left[\frac{1}{\tau_\phi}+\frac{1}{\tau_s}\right]\right) - \ln\left(\frac{\tau}{b}\left[\frac{1}{\tau_\phi}+\frac{1}{\tau_s}\right]\right) + \frac{1}{2}\psi\left(\frac{1}{2}+\frac{\tau}{b}\left[\frac{1}{\tau_\phi}+\frac{2}{\tau_s}\right]\right) - \frac{1}{2}\ln\left(\frac{\tau}{b}\left[\frac{1}{\tau_\phi}+\frac{2}{\tau_s}\right]\right) - \frac{1}{2}\psi\left(\frac{1}{2}+\frac{\tau}{b}\frac{1}{\tau_\phi}\right) + \frac{1}{2}\ln\left(\frac{\tau}{b}\frac{1}{\tau_\phi}\right). \quad (5)$$

Another case is the linear in quasimomentum splitting of the energy spectrum. According to Ref. 41 (see also comments in Ref. 42) $\Delta\sigma(b)$ in this case has the form

$$\frac{\Delta\sigma(b)}{G_0} = \frac{1}{2}\left[\sum_{n=1}^{\infty}\left\{\frac{3}{n} - \frac{3a_n^2 + 2a_n b_s - 1 - 2(2n+1)b_s}{(a_n+b_s)a_{n-1}a_{n+1} - 2b_s[(2n+1)a_n - 1]}\right\} - \frac{1}{a_0} - \frac{2a_0 + 1 + b_s}{a_1(a_0+b_s) - 2b_s} - 2\ln(b_\phi + b_s) - \ln(b_\phi + 2b_s) - 3C - S(b_\phi/b_s) - \Psi(1/2+b_\phi) + \ln b_\phi\right], \quad (6)$$

where $C \approx 0.57721$ is the Euler constant, $b_\phi = b\,\tau/\tau_\phi$, $b_s = b\,\tau/\tau_s$, $a_n = n + 1/2 + b_\phi + b_s$, and $S(b_\phi/b_s)$ is the b-independent function

$$S(x) = \frac{8}{\sqrt{7+16x}}\left[\arctan\frac{\sqrt{7+16x}}{1-2x} - \pi\Theta(1-2x)\right]$$

with $\Theta(y)$ as the Heaviside step function. Expressions (5) and (6) have been derived under assumption that the conductivity is very high, $\sigma \gg G_0$. When it is not the case, one should regard the second-order quantum corrections. To take them into account we have multiplied the right-hand side of both expressions, Eqs. (5) and (6), by the factor $1 - 2G_0/\sigma$ as it has been done for the case of slow spin relaxation in Ref. 43.

In Fig. 7(a), we demonstrate the results of the fitting procedure for $\sigma = 9.75\,G_0$ carried out within the magnetic-field range $b = 0$–0.3 with the use of τ_ϕ and τ_s as the fitting parameters. It is clearly seen that Eq. (6) does not describe the experimental data, while Eq. (5) gives very good agreement. Such the agreement is observed at all temperatures from 1.3 to 4.2 K over the conductivity interval from $5\,G_0$ to $25\,G_0$. Therewith, the temperature dependences of the fitting parameters τ_ϕ and τ_s corresponding to the phase and spin relaxation times, respectively, are reasonable. Again, τ_ϕ demonstrates behavior close to the $1/T$ law, while τ_s is temperature independent within the limits of our accuracy [see Fig.7(b)] typical for the degenerate gas of carriers.

C. Overview of entire conductivity range, σ = (5–130) G_0

Let us now inspect how the results obtained within the different conductivity ranges dovetail into one another. The τ_ϕ values found for different conductivity regions as described above are graphed as a function of the conductivity in Fig. 8(a). The values of the interference correction at $B = 0$ calculated

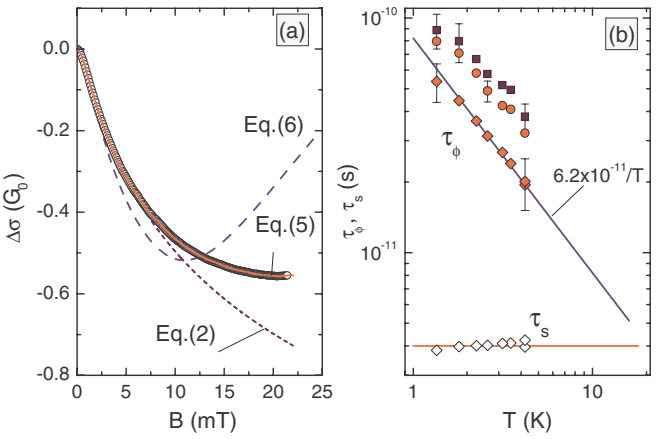

FIG. 7. (Color online) (a) The magnetoconductivity plotted as a function of the magnetic field for $\sigma = 9.75\,G_0$ ($B_{tr} = 62$ mT) at $T = 1.35$ K. The symbols are the data, and the lines show the results of the fitting procedure by the different expressions. (b)- Temperature dependences of τ_ϕ and τ_s obtained with the help of Eq. (5) (diamonds) and Eq. (2) within two magnetic field ranges: $b = 0$–0.05 (circles) and $b = 0$–0.1 (squares).

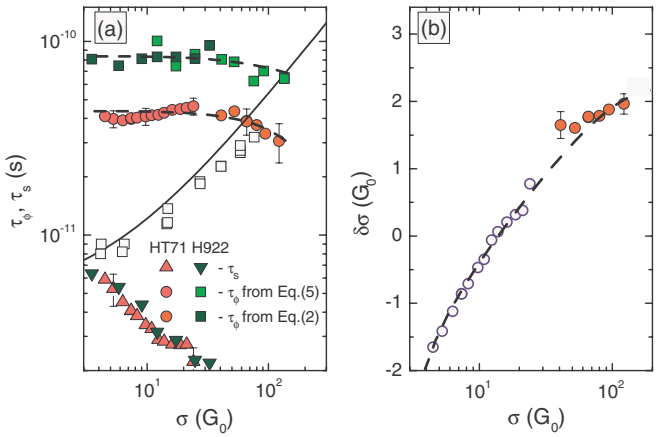

FIG. 8. (Color online) (a) Values of τ_ϕ and τ_s plotted against the conductivity for $T = 1.35$ K for the structures HT71 and H922. The line is calculated according to Ref. 28. The open squares are the experimental results obtained in Ref. 43 on the sample H451 with GaAs/$In_{0.2}Ga_{0.8}$As/GaAs quantum well. (b) Values of interference corrections at zero magnetic field found from Eq. (1) (solid circles) and Eq. (7) (open circles) as a function of the conductivity for $T =$ 1.35 K, structure HT71. The dashed lines in both panels are provided as a guide to the eye.

from Eq. (1) at high conductivity, $\sigma > 20\,G_0$, and from the expression

$$\frac{\delta\sigma(0)}{G_0} = -\frac{1}{2}\ln\frac{\tau}{\tau_\phi} + \ln\left(\frac{\tau}{\tau_\phi}+\frac{\tau}{\tau_s}\right) + \frac{1}{2}\ln\left(\frac{\tau}{\tau_\phi}+\frac{2\tau}{\tau_s}\right) \tag{7}$$

at lower conductivity, are plotted in Fig. 8(b). It is seen that both τ_ϕ versus σ and $\delta\sigma(0)$ versus σ data plots obtained by the two different methods within the low- and high-conductivity regions fall on the smooth curves matching well near $\sigma \simeq 30\,G_0$. Namely these values of $\delta\sigma$ at $B = 0$ have been used to shift the experimental dependences $\Delta\sigma(b)$ in the vertical direction in Fig. 3. An essential feature evident from Fig. 8(a) is that the fitting parameter τ_ϕ does not practically depend on the conductivity over the whole conductivity range from $\sigma \simeq 5\,G_0$ to $\sigma \simeq 130\,G_0$. Such the behavior differs qualitatively from that observed in conventional A_3B_5-based 2D electron systems. For instance, the dephasing time found experimentally in GaAs/$In_{0.2}Ga_{0.8}$As/GaAs single quantum well heterostructures increases about five times over the same conductivity range,[43] which accords well with the theoretical prediction[28] [see line and open squares in Fig. 8(a)].

As already mentioned above the crossover to the positive magnetoconductivity evident at B_c can result from other mechanisms; that is, only the negative magnetoconductivity at $B < B_c$ is caused by suppression of the electron interference, while another unknown mechanism is responsible for the positive magnetoconductivity at $B > B_c$. Then, Eq. (2) rather than Eq. (5) should be used to obtain the value of τ_ϕ at low conductivity $\sigma < 20\,G_0$ as took place for $\sigma > 20\,G_0$. The fitting range should be restricted in this case by the field lower than B_c. The result of such a data treatment for $\sigma = 9.75\,G_0$ is presented in Fig. 7(a) by the dotted line. The fit with the use of τ_ϕ and α as the fitting parameters has been made within two magnetic field ranges: $b = 0{-}0.05$ and $b = 0{-}0.1$. The prefactor α obtained from the fit is approximately equal to -0.3 for both cases, which is close to that expected theoretically $\alpha \simeq -0.5\,(1 - 2G_0/\sigma) \simeq -0.4$. The temperature dependence of τ_ϕ is close to $1/T$, while the value of τ_ϕ is somewhat larger than that found with help of Eq. (5) [see Fig. 7(b)]. Analogous results are obtained within whole low-conductivity range down to $\sigma = 5\,G_0$, but, more importantly, the use of Eq. (2) over the entire conductivity range gives the same result: τ_ϕ does not increase with increasing conductivity.

It is pertinent here to direct the reader's attention to the results obtained on the topological insulator Bi_2Se_3 and reported recently in Ref. 44. The authors present the gate voltage dependence of $B_\phi = \hbar/4eD\tau_\phi$ (D is the diffusion coefficient) found from the fit of the experimental magnetoconductivity curves by Eq. (2). It is possible for some V_g values to convert these data to τ_ϕ versus σ dependence. To do this one should know the dependence of the effective mass on the electron density. If one believes that m is constant in respect to n, we find that τ_ϕ in Bi_2Se_3 decreases with the increasing conductivity within the range $\sigma = (50{-}500)\,G_0$. If one naturally supposes that $m \propto \sqrt{n}$ for the linear Dirac-like spectrum, we obtain results analogous to those presented above for a HgTe quantum well: τ_ϕ is practically independent of σ.

Before closing this section, let us to outline possible reasons for the different behaviors of τ_ϕ with changing σ in the 2D systems with conventional parabolic energy spectra and in the systems with complicated spectra like HgTe single quantum wells. First, the parameters τ_ϕ and τ_s found from the fit may not correspond to the true phase and spin relaxation times despite the fact that the standard expressions, Eq. (2) and Eq. (5), fit the experimental magnetoconductivity curves rather well. Another expression, which properly takes into account the peculiarities of the energy spectrum and electron interference in the HgTe 2D systems, should be derived and used. Second, τ_ϕ found from the fit is true or close to that, but inelasticity of the *e*-*e* interaction in the systems with complicated energy spectra depend on conductivity much weaker than that in the conventional systems, or there is a more effective additional mechanism of inelastic phase relaxation in the structures under study that changes the dependence $\tau_\phi(\sigma)$ drastically. However, it remains unclear in the last case why the dephasing time at low conductivity is 5–10 times larger in HgTe quantum well than that in conventional 2D systems, as Fig. 8(a) illustrates.

IV. CONCLUSION

We have studied the interference-induced magnetoconductivity in a single quantum well of gapless semiconductor HgTe with the inverted energy spectrum. It is shown that only the antilocalization magnetoconductivity is observed at relatively high conductivity $\sigma > (20{-}30)\,G_0$. The antilocalization correction demonstrates the crossover from the $0.5\,\ln(\tau_\phi/\tau)$ to $1.0\,\ln(\tau_\phi/\tau)$ behavior with the increasing conductivity, which is interpreted as a result of crossover to the regime of independent contributions of the two chiral energy branches to the weak antilocalization. At lower conductivity $\sigma < (20{-}30)\,G_0$, the magnetoconductivity behaves itself analogously to that in usual 2D systems with fast spin relaxation. It is negative in low magnetic fields and positive in higher ones. We have found that the temperature dependences of the fitting parameters

τ_ϕ corresponding to the phase relaxation times are close to $1/T$ over the whole conductivity range $\sigma = (5\text{–}130)\,G_0$ that is typical for the dirty 2D systems at low temperatures. However, the τ_ϕ value is practically independent of the conductivity, unlike the conventional 2D systems with simple energy spectra, in which τ_ϕ increases with the growing conductivity.

ACKNOWLEDGMENTS

We thank I. V. Gornyi and I. S. Burmistrov for illuminating discussions. This work has been supported in part by the RFBR (Grants No. 10-02-91336, No. 10-02-00481, and No. 12-02-00098).

[1] A. K. Geim, Rev. Mod. Phys. **83**, 851 (2011).
[2] K. S. Novoselov, Rev. Mod. Phys. **83**, 837 (2011).
[3] M. Z. Hasan and C. L. Kane, Rev. Mod. Phys. **82**, 3045 (2010).
[4] X.-L. Qi and S.-C. Zhang, Rev. Mod. Phys. **83**, 1057 (2011).
[5] B. A. Bernevig, T. L. Hughes, and S.-C. Zhang, Science **314**, 1757 (2006).
[6] B. Buttner, C. X. Liu, G. Tkachov, E. G. Novik, C. Brune, H. Buhmann, E. M. Hankiewicz, P. Recher, B. Trauzettel, S. C. Zhang, and L. W. Molenkamp, Nat. Phys. **7**, 418 (2011).
[7] S. Groves and W. Paul, Phys. Rev. Lett. **11**, 194 (1963).
[8] V. A. Volkov and T. N. Pinsker, Zh. Eksp. Teor. Fiz. **70**, 2268 (1976) [Sov. Phys. JETP **43**, 1183 (1976)].
[9] M. I. Dyakonov and A. Khaetskii, Zh. Eksp. Teor. Fiz. **82**, 1584 (1982) [Sov. Phys. JETP **55**, 917 (1982)].
[10] Y. R. Lin-Liu and L. J. Sham, Phys. Rev. B **32**, 5561 (1985).
[11] L. G. Gerchikov and A. Subashiev, Phys. Status Solidi B **160**, 443 (1990).
[12] F. Goschenhofer, J. Gerschütz, A. Pfeuffer-Jeschke, R. Hellmig, C. R. Becker, and G. Landwehr, J. Electron. Mater. **27**, 532 (1998).
[13] N. N. Mikhailov, R. N. Smirnov, S. A. Dvoretsky, Y. G. Sidorov, V. A. Shvets, E. V. Spesivtsev, and S. V. Rykhlitski, Int. J. Nanotechnology **3**, 120 (2006).
[14] X. C. Zhang, A. Pfeuffer-Jeschke, K. Ortner, C. R. Becker, and G. Landwehr, Phys. Rev. B **65**, 045324 (2002).
[15] X. C. Zhang, K. Ortner, A. Pfeuffer-Jeschke, C. R. Becker, and G. Landwehr, Phys. Rev. B **69**, 115340 (2004).
[16] G. M. Gusev, Z. D. Kvon, O. A. Shegai, N. N. Mikhailov, S. A. Dvoretsky, and J. C. Portal, Phys. Rev. B **84**, 121302 (2011).
[17] K. Ortner, X. C. Zhang, A. Pfeuffer-Jeschke, C. R. Becker, G. Landwehr, and L. W. Molenkamp, Phys. Rev. B **66**, 075322 (2002).
[18] G. M. Gusev, E. B. Olshanetsky, Z. D. Kvon, N. N. Mikhailov, S. A. Dvoretsky, and J. C. Portal, Phys. Rev. Lett. **104**, 166401 (2010).
[19] M. König, S. Wiedmann, C. Brüne, A. Roth, H. Buhmann, L. W. Molenkamp, X.-L. Qi, and S.-C. Zhang, Science **318**, 766 (2007).
[20] Z. D. Kvon, E. B. Olshanetsky, E. G. Novik, D. A. Kozlov, N. N. Mikhailov, I. O. Parm, and S. A. Dvoretsky, Phys. Rev. B **83**, 193304 (2011).
[21] E. B. Olshanetsky, Z. D. Kvon, G. M. Gusev, N. N. Mikhailov, S. A. Dvoretsky, and J. C. Portal, JETP Lett. **91**, 347 (2010).
[22] G. Tkachov and E. M. Hankiewicz, Phys. Rev. B **84**, 035444 (2011).
[23] V. A. Larionova and A. V. Germanenko, Phys. Rev. B **55**, 13062 (1997).
[24] S. Hikami, A. I. Larkin, and Y. Nagaoka, Prog. Theor. Phys. **63**, 707 (1980).
[25] H.-P. Wittmann and A. Schmid, J. Low Temp. Phys. **69**, 131 (1987).
[26] B. L. Altshuler and A. G. Aronov, in *Electron-Electron Interaction in Disordered Systems*, edited by A. L. Efros and M. Pollak (North Holland, Amsterdam, 1985), p. 1.
[27] G. M. Minkov, A. V. Germanenko, V. A. Larionova, S. A. Negashev, and I. V. Gornyi, Phys. Rev. B **61**, 13164 (2000).
[28] G. Zala, B. N. Narozhny, and I. L. Aleiner, Phys. Rev. B **64**, 214204 (2001).
[29] W. Knap, A. Zduniak, L. H. Dmowski, S. Contreras, and M. I. Dyakonov, Phys. Status Solidi B **198**, 267 (1996).
[30] C. Castellani, C. Di Castro, P. A. Lee, M. Ma, S. Sorella, and E. Tabet, Phys. Rev. B **30**, 1596 (1984).
[31] A. M. Finkel'stein, Zh. Eksp. Teor. Fiz. **86**, 367 (1984) [Sov. Phys. JETP **59**, 212 (1984)].
[32] R. Raimondi, C. Castellani, and C. Di Castro, Phys. Rev. B **42**, 4724 (1990).
[33] C. Castellani, C. Di Castro, and P. A. Lee, Phys. Rev. B **57**, R9381 (1998).
[34] G. Zala, B. N. Narozhny, and I. L. Aleiner, Phys. Rev. B **65**, 020201 (2001).
[35] I. V. Gornyi and A. D. Mirlin, Phys. Rev. B **69**, 045313 (2004).
[36] G. M. Minkov, A. A. Sherstobitov, A. V. Germanenko, O. E. Rut, V. A. Larionova, and B. N. Zvonkov, Phys. Rev. B **72**, 165325 (2005).
[37] G. M. Minkov, O. E. Rut, A. V. Germanenko, A. A. Sherstobitov, V. I. Shashkin, O. I. Khrykin, and B. N. Zvonkov, Phys. Rev. B **67**, 205306 (2003).
[38] E. M. Baskin, L. N. Magarill, and M. V. Entin, Sov. Phys. JETP **48**, 365 (1978).
[39] A. Dmitriev, M. Dyakonov, and R. Jullien, Phys. Rev. B **64**, 233321 (2001).
[40] V. V. Cheianov, A. P. Dmitriev, and V. Y. Kachorovskii, Phys. Rev. B **70**, 245307 (2004).
[41] S. V. Iordanskii, Y. B. Lyanda-Geller, and G. E. Pikus, Zh. Eksp. Teor. Fiz. **60**, 199 (1994) [JETP Lett. **60**, 206 (1994)].
[42] G. M. Minkov, A. V. Germanenko, O. E. Rut, A. A. Sherstobitov, L. E. Golub, B. N. Zvonkov, and M. Willander, Phys. Rev. B **70**, 155323(2004).
[43] G. M. Minkov, A. V. Germanenko, and I. V. Gornyi, Phys. Rev. B **70**, 245423 (2004).
[44] J. Chen, X. Y. He, K. H. Wu, Z. Q. Ji, L. Lu, J. R. Shi, J. H. Smet, and Y. Q. Li, Phys. Rev. B **83**, 241304 (2011).